



Enhanced acidic dye adsorption onto the dendrimer-based modified halloysite nanotubes

Farnaz Shahamati Fard, Somaye Akbari*, Elmira Pajootan, Mokhtar Arami

Textile Engineering Department, Amirkabir University of Technology, 424 Hafez Ave, Tehran, Iran, email: farnaz_fard@aut.ac.ir (F. Shahamati Fard), Tel. +98 2164542614; Fax: +98 2166400245; emails: akbari_s@aut.ac.ir (S. Akbari), pajootan@aut.ac.ir (E. Pajootan), arami@aut.ac.ir (M. Arami)

Received 3 October 2015; Accepted 20 February 2016

ABSTRACT

In this study, amine-terminated dendritic functional groups were grown on the surface of Halloysite Nanotubes (HNTs) to improve their adsorption tendency towards the anionic dye molecules. HNTs were first silanized by (3-Aminepropyl) triethoxysilane, and then amine dendritic groups were added via divergent synthesis from zero to third generation by repeating the Michael addition of methyl acrylate and amidation of the esters groups with ethylenediamine. In fact, amine groups of APTES act as a core for growing of dendritic structure in divergent synthetic route. Field emission scanning electron microscopy, energy dispersive X-ray spectroscopy analysis, and Fourier transform infrared spectroscopy were used to characterize the modified HNTs. The adsorption of C.I. Acid Red 1 (AR1) and C.I. Acid Red 42 (AR42) was investigated and the effect of initial dye concentration, pH, adsorbent dosage, and temperature was studied. The adsorption isotherm and kinetic data followed the Langmuir and pseudo-second-order equations, respectively. The maximum removal efficiencies of 93–94% were achieved at pH 3 for AR1 and AR42, respectively, while the pure HNTs revealed only 9–13% of removal.

Keyword: Halloysite nanotubes; Dendrimer; Amine-terminated functional groups; Equilibrium parameters

1. Introduction

Halloysite nanotubes (HNTs) are natural-mineral clay with hollow nanotubular structure [1]. HNTs possess a unique lumen form in physical structure. The size of HNTs lumen is usually in the range of 1–15 nm, their external and internal diameters are 50–70 nm and 10–30 nm, and the length of HNTs is within the range of 800 ± 300 nm [2]. HNTs are abundant in many countries such as China, USA, Brazil,

and France [3], and they have notable importance in material science due to their special features of large surface area, unique tubular structure, high porosity, high length-to-diameter ratio [3], and high receptor surface chemistry, which have made this nanomaterial to be utilized as a proper adsorbent, container catalyst, and nanofiller for composite [4]. HNTs are one of the cheapest existing adsorbents [5–8]. This substance naturally contains aluminosilicate nanotubes with a 1:1 Al:Si ratio and a stoichiometry of $\text{Al}_2\text{Si}_2\text{O}_5(\text{OH})_4 \cdot n\text{H}_2\text{O}$. There are mainly two structures for HNTs: the anhydrous form with an interlayer of 7 Å, and its hydrated

*Corresponding author.

form with expanded interlayer spacing of 10 Å as a result of water prevailing the inter lamellar space [9]. Halloysite tubes consist of octahedral sheets of Al–OH groups on the internal surface, and siloxane groups (Si–O–Si) on the external surface. This variances have led to a negatively charged outer surface and a positively charged inner lumen at pH range of 2–8 [10,11].

HNTs have been used as additive to fortify the mechanical performance of polymers [12], to increase molecular adsorption [13,14], in nanocomposite [2], enzyme immobilization [15,16], nano filler [17], carrier [18], improving antifouling properties [19], molecular encapsulation [11], storage and transport [11], and catalyst or catalyst support in chemical reactions [20,21]. The most important advantage of HNTs as a mineral adsorbent compared to the other minerals like bentonite is related to the lumen of their internal structure which allows them to go under different functionalization treatments.

To improve more application of HNTs, various modification methods of HNTs have been reported in literature like HNTs-octadecylphosphonic [10], HNTs-chitosan [22], HNTs-lactic acid [23], HNTs-HDTMA [24], and HNTs-APTES [3,25]. One of the most promising methods to increase the abundant hydrophilic groups on the surface of HNTs is by grafting the amine group, which can even make the amine-terminated HNTs more proper for the catalytic applications [2,21].

APTES can be used to modify and functionalize HNTs by amine propyl groups [25]. AlOH groups of internal walls and AlOH and SiOH groups at the edges and external surface of HNTs can all be targeted during the modification process [10,26,27]. The formation of hydrogen bond between the hydroxyl and amine groups on the inner walls or edges and grafting of amine groups directly onto all surfaces of HNTs are the possible mechanisms of binding APTES to HNTs [25,28,29].

Amine groups can be introduced to the surface of HNTs by amine-terminated dendritic groups. Dendrimers are class of polymers that possess notable properties and applications. These well-known polymers are defined as tree-dimensional structures by versatile chemical properties. Dendrimers have different functional end groups and the number of these groups can be controlled by choosing a proper synthetic method and generation [30]. This attractive class of polymer can be used in drug delivery in medicine [31], catalysis [32], modules, and strength reinforcement of resins [2].

Dendritic materials can also be used for the removal of contaminants from wastewaters. The removal of color from dye containing wastewaters

such as textile, dyeing, printing, and other related industries has long been a serious environmental problem in the world [33,34]. The wastewater generated usually contains substances that are severely harmful to the environment. Textile dyeing is a chemically intensive process which consumes large quantities of water [35]. In a typical dyeing process, 50–100% of dye is fixed on the fiber, and the unfixed dyes are discharged into the dye-baths or into the wastewater from the subsequent textile-washing operations [35]. To comply with stringent discharge limits, multi-step and complicated treatment is usually required. There are different methods available for dye removal like biological treatment [36], coagulation/flocculation [37–39], chemical oxidation and photocatalysis [40], ozone treatment [41], membrane processes, and adsorption [42]. Adsorption is a highly efficient and low-cost process for the treatment of polluted waters [43,44]. Numerous types of adsorbent such as activated carbon [45,46], silica [47], zeolite [48], kaolinite [49], and bentonite [50] have been employed for the adsorption techniques, but in some cases the adsorbents are so expensive or in other cases they are inapplicable. These investigations have acclaimed the researchers to find cheaper materials as adsorbents.

This study demonstrated that the particular chemical structure of HNTs have high potential for the functionalization. Therefore, the step by step synthesis of amine-terminated dendritic groups on the surface of HNTs has been performed. In this regard, HNTs were first acidified and amine functionalized in HCl and APTES solution, respectively. Then, the generation 1–3 of dendrimer was synthesized on the surface of HNTs. The amine functionalized HNTs have the potential to be used as an efficient adsorbent for the removal of dyes from colored wastewaters, so they were employed as adsorbent to remove two acid dyes: C.I. Acid Red 1 (AR1) and C.I. Acid Red 42 (AR42). The influence of various generations of the synthesized dendrimer on the surface of HNTs was discussed, and the effect of other key parameters including pH, adsorbent dosage, dye concentration, temperature, and time on the adsorption efficiency was evaluated. The isotherm, kinetic, and thermodynamic parameters were also calculated and reported.

2. Materials and methods

2.1. Chemicals and materials

The HNTs (diameter: 80 nm) were kindly donated from Delta-Dolsk Company, Poland. Aminepropyltriethoxysilane (APTES), methyl acrylate (MA), ethanol,

ethylene diamine (EDA), diethyl ether, and all the other chemicals were of laboratory reagent grade and they were supplied from Aldrich. AR1 and AR42 were purchased from Ciba and their structures, formula and molecular weight are defined in Table 1.

2.2. Synthesis of HNTs-G₃ via divergent synthetic route

The divergent process of dendrimer synthesis onto the HNTs is explained in detail as follows:

First, HNTs were purified in HCl solution (35%) for 24 h using a magnetic stirrer, and then they were washed three times with distilled water to reach a constant pH value. The purified HNTs were poured on a clean substrate and then dried in oven at 60°C for 24 h (step 1). The acidified HNTs (30 g), toluene (150 mL), and APTES (40 mL) were refluxed for 12 h at 60°C to introduce amine groups on the HNTs (step 2). The solution was washed with diethyl ether, ethanol and methanol, each for five times to remove impurities and then dried at 60°C.

HNTs-APTES (31.25 g) were modified by Michael addition of MA (32 mL in ethanol solution at 60°C), which were synthesized by APTES onto HNTs. After 24 h, the solution was washed with methanol and then dried at 60°C (step 3). The last step (step 4) to synthesize HNTs-G₁ was the amidation of ester groups with EDA. EDA was added to methanol and HNTs-MA solution at 60°C for 24 h in to the flask. The mixture was washed as same as step 3. Finally, steps 3 and 4 were repeated two times to achieve HNTs-G₃. Fig. 1

represents the synthesis strategy for the functionalized HNTs from G₀ to G₃. Due to the mechanism of grafting APTES onto the HNTs [25,28,29], dendritic structure were grown on the amine groups of HNTs-APTES. On the other hand, amine groups of APTES act as a core for growing of dendritic structure.

2.3. Adsorption process

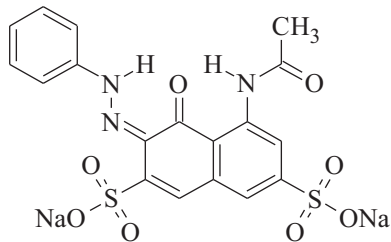
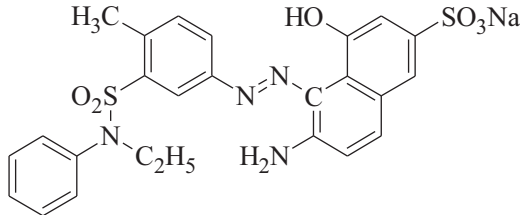
Dye solutions were prepared (250 mL) in a defined concentration and pH of solutions was adjusted using H₂SO₄ (0.1 N) and NaOH (0.1 N). A specified dosage of adsorbent was added to the colored solution stirring on a magnetic stirrer to start the adsorption process. Samples were taken from the solution at different time intervals and centrifuged for 10 min at 5,000 rpm. Finally, the absorbance of the samples was measured by UNICO 2100 spectrophotometer. The amount of dye adsorbed per gram of HNTs (mg g⁻¹) and dye removal efficiency were calculated from Eqs. (1) and (2), respectively.

$$q_t = V(C_0 - C_t)/W \quad (1)$$

$$\text{Dye removal (\%)} = \frac{(C_0 - C_t) \times 100}{C_0} \quad (2)$$

where q_t is adsorption capacity (mg g⁻¹), C_0 and C_t are the dye concentration before and after the adsorption (mg L⁻¹), V is the volume of solution (L), and W is the mass of adsorbent (g).

Table 1
Structure and characteristics of dyes

C.I. generic name	Structure	Formula	λ_{Max}	M _w (g/mol)	Number of sulfonate groups
C.I. Acid Red 1		C ₁₈ H ₁₃ N ₃ Na ₂ O ₈ S ₂	506	509.42	2
C.I. Acid Red 42		C ₂₅ H ₂₂ N ₄ Na ₁ O ₅ S ₂	516	589	1

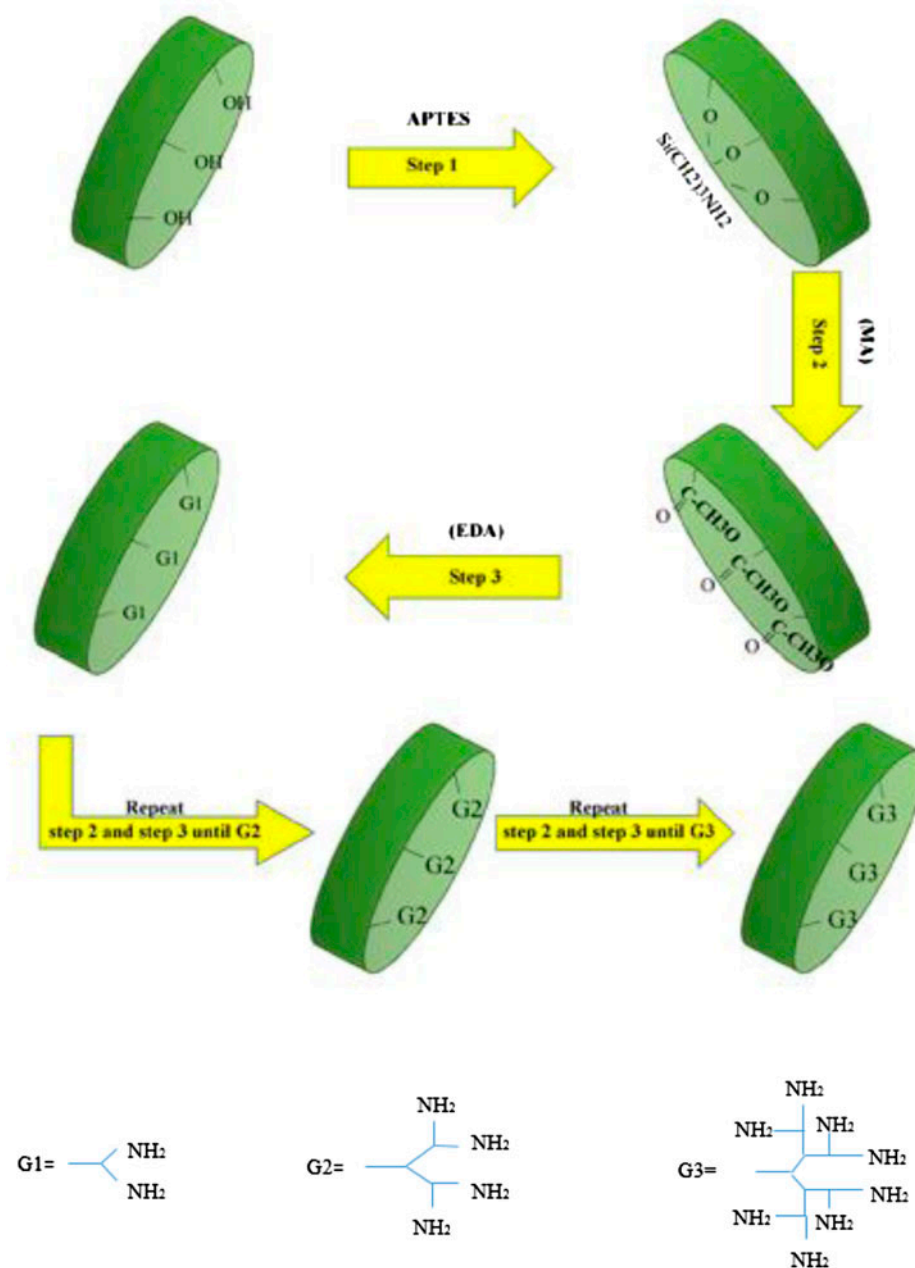


Fig. 1. The synthesis steps of amine-terminated HNTs.

2.4. Characterization

Characterization of HNTs before and after the modification was studied using field emission scanning electron microscopy (FESEM), energy dispersive X-ray spectroscopy analysis (EDS), and Fourier transform infrared (FTIR) analysis. The surface morphology of the adsorbents was investigated by FESEM (FESEM, S-4160 Hitachi Company).

FTIR spectra of raw and modified HNTs from generation 1–3 were recorded between 4,000 and 400 cm^{-1} using a Nicolet 670 FTIR spectrophotometer. Nominal resolution for all spectra was 4 cm^{-1} , and there were 32 scans for each spectrum. The samples were ground with KBr crystals, and the mixtures were pressed into pellets for IR measurements. All the spectra were normalized using the intensity of the band at 538 cm^{-1} ,

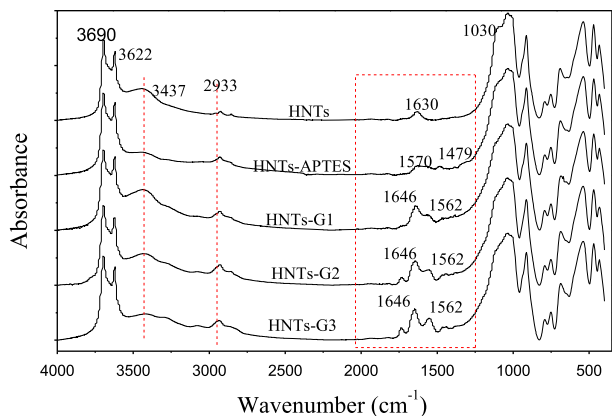


Fig. 2. FTIR spectra of HNTs through the modification steps.

which is assigned to the Al–O–Si as an internal standard [25,51].

3. Results and discussion

3.1. Structural characterization of HNTs

Fig. 2 and Table 2 show the FTIR spectra and the corresponding functional groups assigned to each peak in the structure of HNTs, HNTs-APTES, HNTs-G₁, HNTs-G₂, and HNT-G₃. According to Fig. 2, the

peaks at 3,622–3,690 cm⁻¹ are ascribed to the stretching vibration of inner-surface Al–OH groups [52]. The peak appeared at 1,630 and 914 cm⁻¹ indicated OH bending vibration groups relating to the interlayer water and inner surface hydrogen group of HNTs. The peak relating to the stretching bond of Si–O appeared at 1,030 cm⁻¹. The corresponding peaks located at 532 and 475 cm⁻¹ are the bending vibrations of Al–O–Si and Si–O–Si [9,51].

Modified HNTs via APTES exhibited new peaks such as stretching and scissoring CH₂ at 2,929 and 1,490 cm⁻¹, and N–H stretching vibration at 3,402 cm⁻¹ attributed to the addition of primary amines groups [25,53]. The intensity of OH peak at the range of 3,690–3,622 decreased for HNTs-APTES, but it showed a broad peak at 3,360 cm⁻¹ corresponding to the overlapped OH and NH₂ groups [25]. The new peak at 1,562 cm⁻¹ was assigned to bending N–H groups [25], and the peak at 1,479 cm⁻¹ was attributed to CH₂ bending vibration [6]. All of these observations indicated that HNTs-APTES has been synthesized successfully.

When HNT-G₁ is synthesized, some new peaks are appeared in the spectrum. These new peaks at 3,300–3,500 cm⁻¹ can be related to N–H stretching vibration [25]. The peaks appeared at 2,925 and 2,877, 1,646, and 1,562 cm⁻¹, are corresponding to the stretching vibrations of CH₂, N–H bending vibrations and C–N bond,

Table 2

FTIR spectra analysis of HNTs, HNTs-APTES, HNTs-G₁, HNTs-G₂, and HNTs-G₃

Wavenumber (cm ⁻¹)	Functional group	Refs.
3,690–3,622	Stretching vibration of inner surface Al–OH	[6,51,52]
3,618	OH stretching of inner hydroxyl group	[25]
3,402	Stretching vibration of N–H	[25,53]
3,300–3,360	Asymmetric and symmetric stretching of NH ₂	[25]
2,929	Asymmetric stretching of CH ₂	[6,25]
2,852	Symmetric stretching of CH ₂	[51]
2,025	Si–H group stretching	[53]
1,732	Stretching vibration of C=O ester groups	[62]
1,646	Deformation (bending) of N–H	[6,25]
1,630	OH deformation of water	[6,25]
1,562	Vibration bond of C–N	[25]
1,479	Bending vibration of CH ₂	[6]
1,384	Deformation (wagging) of C–H	[25]
1,330	Deformation (scissoring) of Si–CH	[25]
1,266	Deformation (scissoring) of CH ₃	[25]
1,085	In plan Si–O stretching	[6,25,51,53]
1,030	Perpendicular Si–O stretching	[25]
1,000	Si–O group at the surface of HNTs	[25,51,52]
914	OH bending vibration of inner hydroxyl group	[25,51,52]
538	Al–O–Si deformation	[6,25,51,52]
475	Si–O–Si deformation	[6,25,51,52]

respectively. The intensity of modified HNTs are higher in the order of HNTs-G₃, HNTs-G₂, and HNTs-G₁ [6,25,51]. The appearance of these new peaks and their increased intensities confirm the successful modification.

The FESEM images of all the modified HNTs were analyzed. For the similarity of the images only FESEM images of pure HNTs and HNTs-G₃ are illustrated in Fig. 3. The tubular structure of HNTs shown in these images indicates that the morphology of HNTs remains unchanged after the modification steps. The EDS analysis of HNTs before and after the modification process is shown in Fig. 4. It detects iron, aluminum, silicon, oxygen, and nitrogen elements in the structure of HNTs samples. It is evident that the weight percentage of nitrogen increases after the modification with APTES and synthesis of each dendrimer generation onto HNTs. The nitrogen weight (%) increased from 3.02% for raw HNTs to 9.32% for HNTs-G₃, which confirms the synthesis of amine groups onto HNTs.

3.2. Evaluation of adsorption process

3.2.1. Effect of generation

The influence of various generations of dendritic structure synthesized onto the surface of HNTs was investigated on dye removal efficiency (Fig. 5). The experimental results show that by increasing the generation, dye removal (%) increase slightly. As the generation of synthesized dendrimer grows, the number of amine-terminated groups on the surface of HNTs increases which amplifies the adsorption rate

and capacity. The removal percentages of raw HNTs for AR1 and AR42 are only 9–13.8%, which are associated with the negative hydroxyl functional groups at the inner surface of HNTs. Also, both anionic dyes and HNTs are negatively charged, which leads to the repulsion forces between the adsorbent and adsorbate. When HNTs are modified with APTES, the removal efficiencies increase due to the addition of amine groups to the structure of HNTs, but it can be seen that by further synthesis of amine-terminated groups, more positive groups are located onto the surface of HNTs, and by increasing the generation, the number of amine groups are increased, which was confirmed by EDS analysis [54]. This results in significantly higher values of removal (%) at higher generation, 82, 83, and 94% for AR1 and 69, 75, and 87% for AR42. Higher removal efficiencies of AR1 rather than AR42 can also be due to the existence of more sulfonate groups in its structure [55].

3.2.2. Effect of pH

One of the most important parameters that affect the dye removal is pH of the solution. In order to investigate this factor, five different pH values were elected and dye removal was determined at pH 3, 5, 7, 9, and 11, while the other parameters were kept constant. The dye concentration was 25 and 4 mg L⁻¹ of HNTs-G₃ sorbent was used at room temperature. It was found as shown in Fig. 6 that high removal efficiencies of 94 and 87% was obtained for AR1 and AR42, respectively, at pH 3, but experimental results

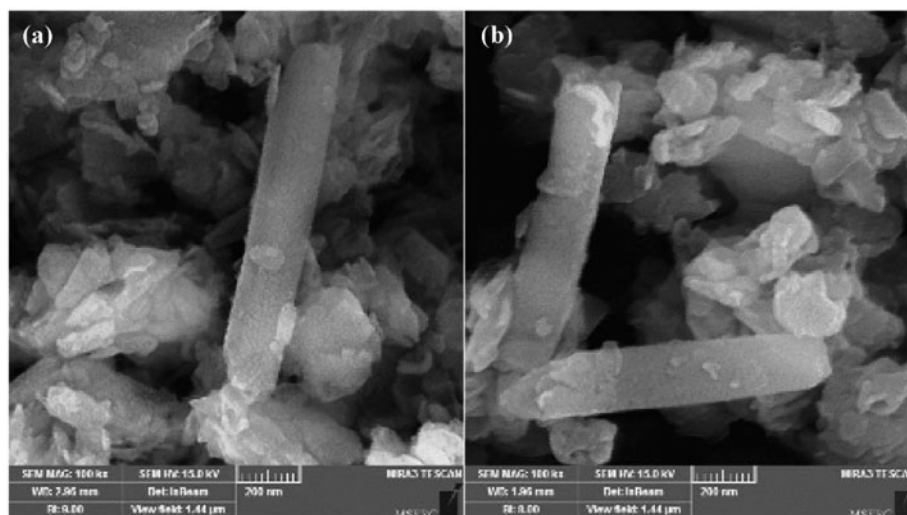


Fig. 3. FESEM images of (a) HNTs and (b) HNTs-G₃.

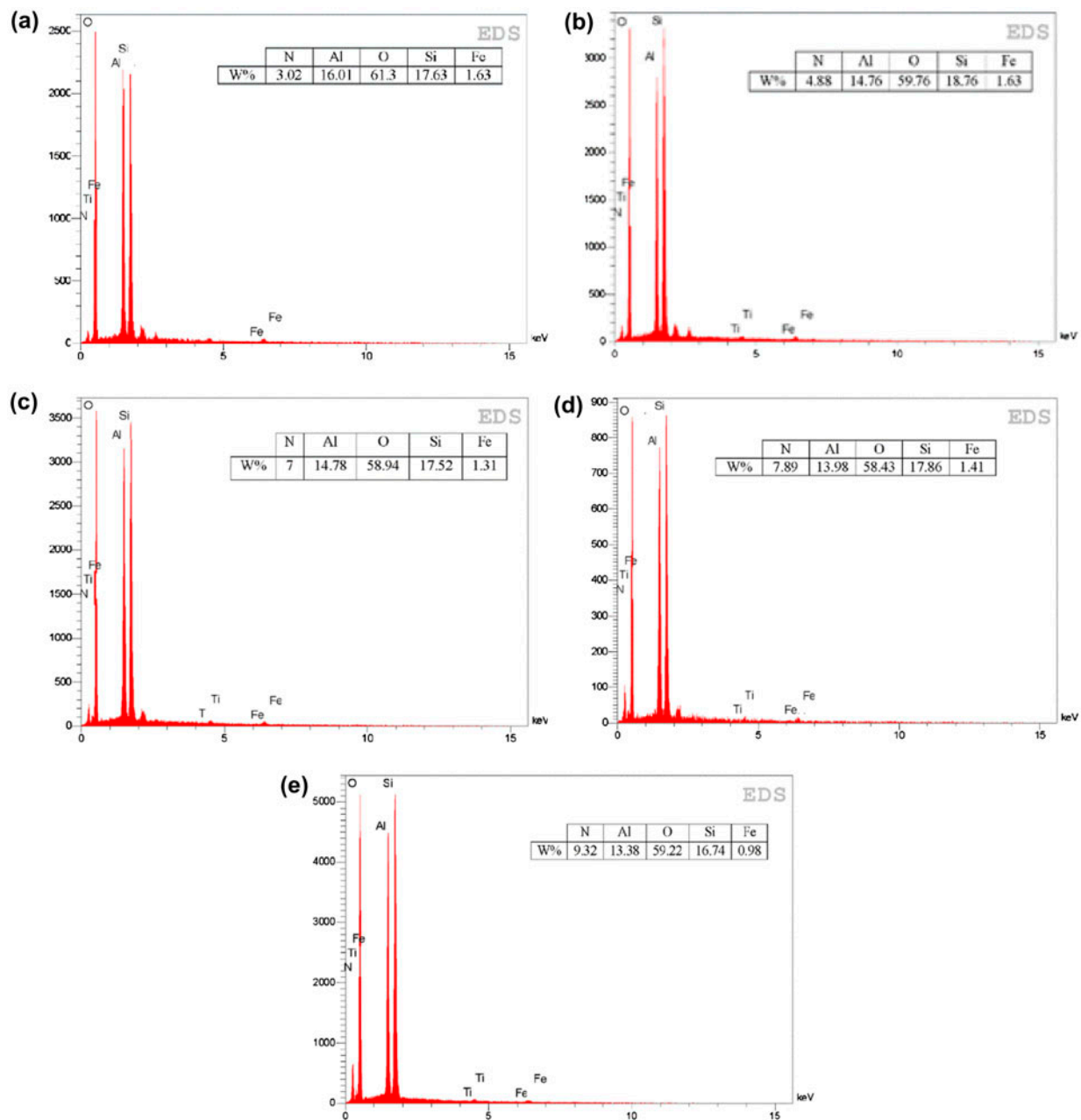


Fig. 4. EDS analysis of (a) HNTs, (b) HNTs-APTES, (c) HNTs-G₁, (d) HNTs-G₂, and (e) HNTs-G₃.

illustrated low dye removal (9–13.8%) for both acidic dyes using raw HNTs. Besides, at pH values above 5.0 there was a decreasing trend in dye removal (%), and at high pH values, the dye removal was very low (approximately 7% at pH 11).

Since the surface of HNTs-G₃ is covered with positively charged amine groups and the dye molecules contain negative charges because of their functional groups such as OH⁻ and SO₃⁻, the removal efficiencies are higher at acidic media due to the electrostatic attraction forces. At higher pH values,

OH⁻ existed in solution shows attraction to the surface amine groups and compete with the anionic dye molecules and consequently, decrease the removal efficiency [56].

3.2.3. Effect of adsorbent dosage

The effect of adsorbent dosage was investigated by the addition of different amount of HNTs-G₃ (0.4–0.8 g L⁻¹) into the solution (Fig. 7). The removal percentage increased when the adsorbent dosage

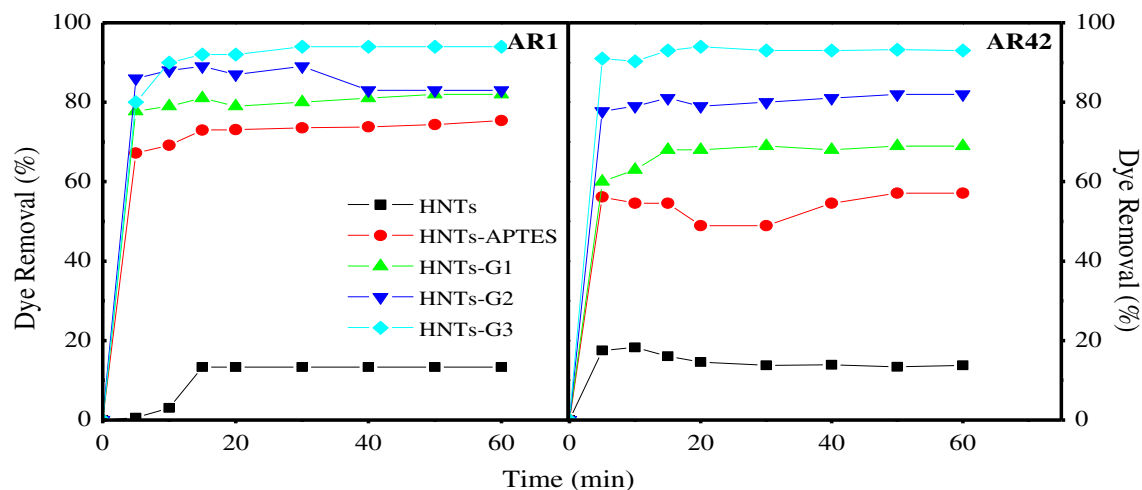


Fig. 5. Effect of generation on AR1 and AR42 removal (%) (Initial dye concentration: 25 mg L^{-1} , adsorbent dosage: 0.7 g L^{-1} for AR42 and 0.5 g L^{-1} for AR1, pH 3).

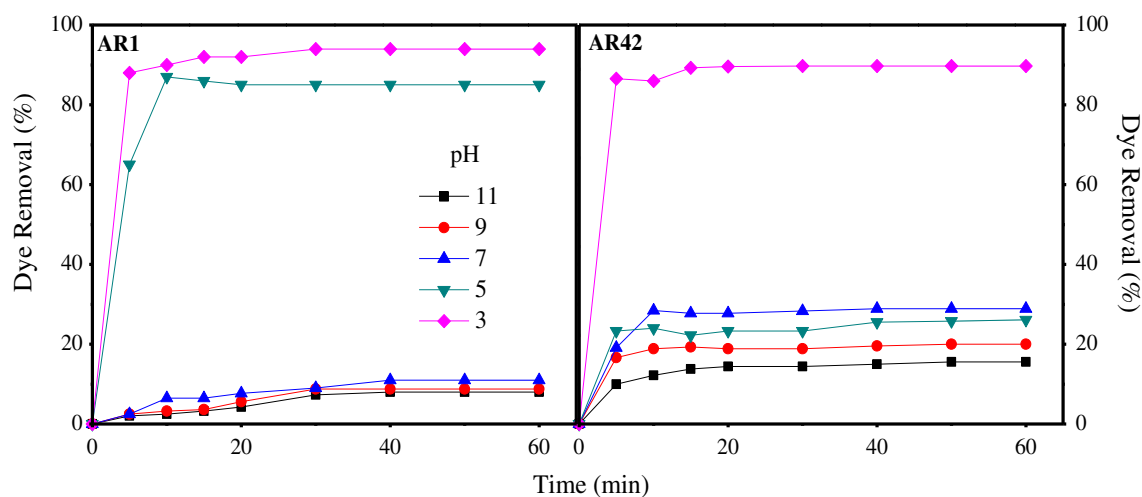


Fig. 6. Effect of pH on AR1 and AR42 removal (%) by HNTs-G₃ (Initial dye concentration: 25 mg L^{-1} , adsorbent dosage: 0.7 g L^{-1} for AR42 and 0.5 g L^{-1} for AR1, generation: 3).

increased. This can be related to the specific surface area and terminal active sites of adsorbent, which are increased by increasing the adsorbent dosage, and consequently enhance the adsorption efficiency [57]. The optimum adsorbent dosage was obtained 0.7 g L^{-1} for AR42 and 0.5 g L^{-1} for AR1.

The results indicated that the optimum dosage of adsorbent to reach the sufficient removal (%) differs from AR1 to AR42, which may be dependent on dye structures. According to Table 1, higher number of SO_3^- groups exists in the structure of AR1, which leads to the stronger electrostatic attraction forces between the dye molecule and adsorbent and thus, higher

removal efficiency is obtained rather than AR42 which contains one sulfonate group.

3.2.4. Effect of initial dye concentration

The effect of initial dye concentration is shown in Fig. 8. Various concentrations of dye were examined in the range of $25\text{--}100 \text{ mg L}^{-1}$. Obviously, increasing the dye concentration inclined to decrease the removal percentage. This adverse correlation is assigned to the unavailable adsorption sites [58]. In adsorption process vacant sites of adsorbent are saturated and dye molecules aggregate on the surface of adsorbent, which will

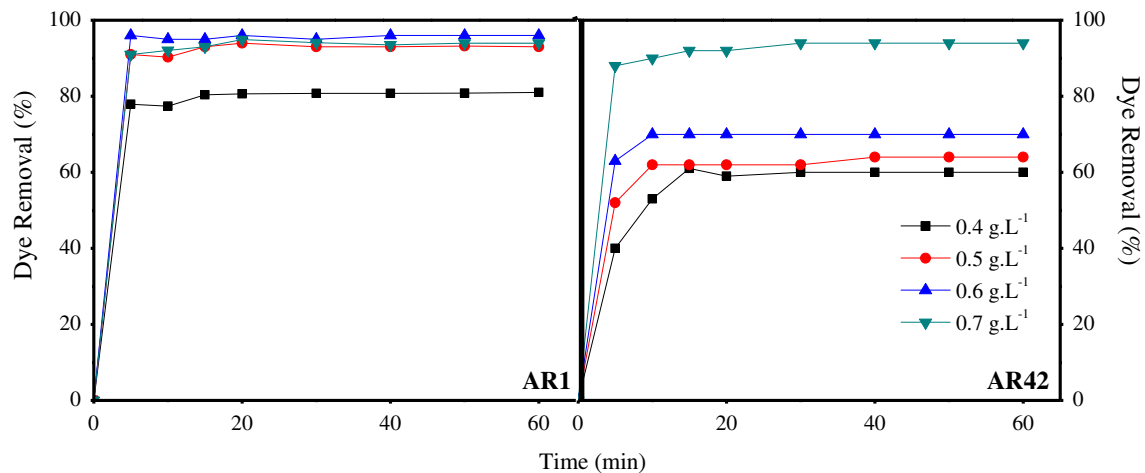


Fig. 7. Effect of adsorbent dosage on AR1 and AR42 removal (%) by HNTs-G₃ (Initial dye concentration: 25 mg L⁻¹, generation: 3, pH 3).

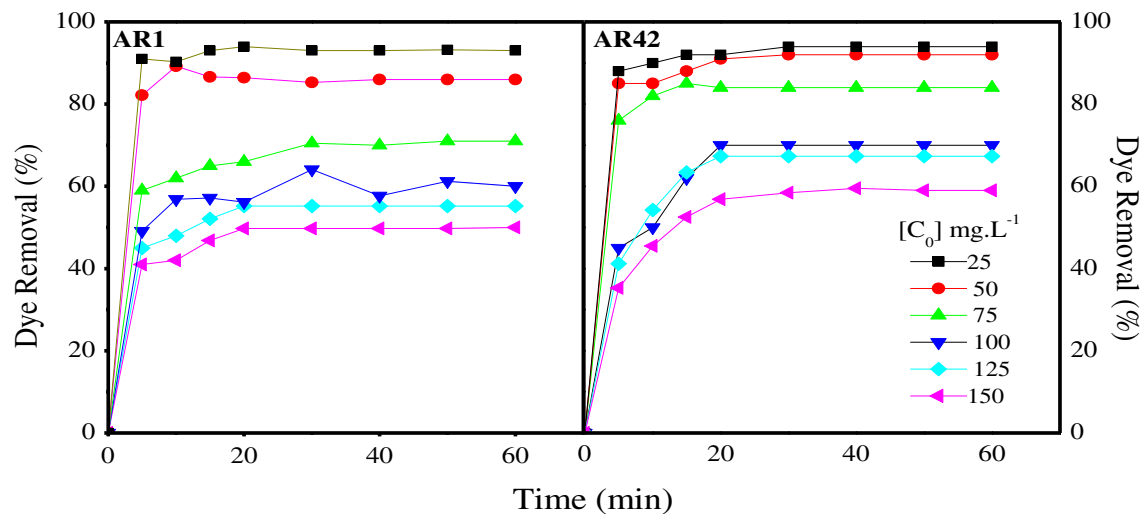


Fig. 8. Effect of initial dye concentration on AR1 and AR42 removal (%) by HNTs-G₃ (Adsorbent dosage: 0.7 g L⁻¹ for AR42 and 0.5 g L⁻¹ for AR1, generation: 3, pH 3).

cause the essential driving force not to overcome the mass transfer between aqueous and solid phase, and thus the removal (%) of AR1 and AR16 decreases [57].

The adsorption capacity is a valuable factor for the evaluation of the adsorbent performance. The experimental results indicate that the adsorption capacity of HNTs-G₃ increases significantly from 46.39 and 32.85 to 140.2 and 114 (mg g⁻¹) for AR1 and AR42 with the increase in the initial dye concentration from 25 to 150 (mg L⁻¹), respectively.

3.2.5. Desorption studies

Regeneration of the modified HNTs was investigated by adsorption/desorption experiments. Adsorp-

tion experiments were carried out using 0.125–0.175 g of HNTs-G₃ for AR1 and AR42 solutions at optimum condition. Then, the dye loaded adsorbent was dried at 60°C for 24 h. Desorption processes were performed at various pH values of 3, 5, 7, 9, and 11. The results in Fig. 9 illustrate that the desorption increases at higher pH values. This may be attributed to the electrostatic behavior of positive and negative charges [51]. Thereby, the competition between OH⁻ and dye molecules tends to increase the desorption rate from the modified HNTs surface at high pH values. It was observed that desorption efficiency of AR1 was higher than AR42, which can be due to the number of their sulfonate groups. Dye molecules with more sulfonate groups revealed higher desorption percentages from

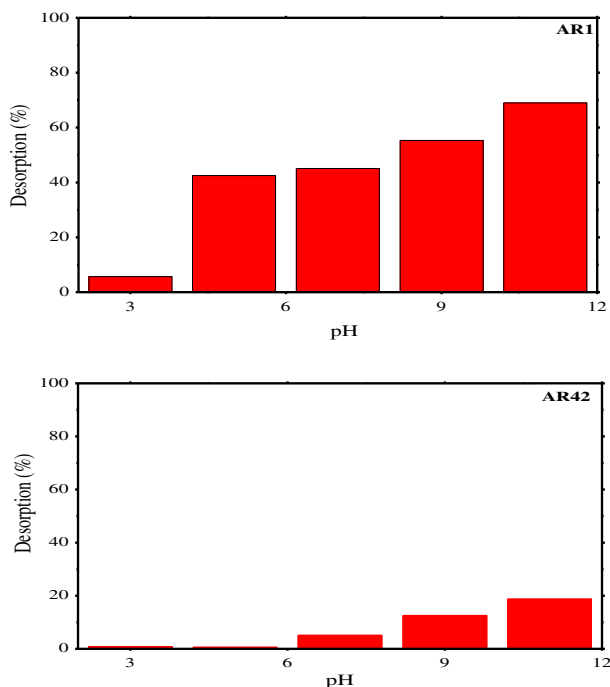


Fig. 9. Desorption study of AR1 and AR42 at different pH.

the modified HNTs surface. Desorption percentages at pH 11 were 68.98 and 18.75% for AR1 and AR42, respectively.

3.3. Adsorption isotherms

Adsorption isotherm models explain the reaction between the adsorbent and adsorbates. These isotherms play an important role in designing an adsorption system. Here, the equilibrium analysis by different models such as Langmuir, Temkin, and Freundlich is described [58].

3.3.1. Langmuir isotherm

The Langmuir adsorption is defined by the monolayer adsorption, and the whole adsorption sites are equivalent for energy and adsorption tendency. The

linear form of Langmuir equation is represented as Eq. (3):

$$\frac{C_e}{q_e} = \frac{1}{K_L Q_m} + \frac{C_e}{Q_m} \tag{3}$$

where C_e is the concentration of each dye at equilibrium condition (mg L^{-1}) and q_e is the amount of dye adsorbed per unit mass of HNTs- G_3 (mg g^{-1}). Q_m is the hypothetical maximum amount of adsorption capacity for adsorbent (mg g^{-1}) and K_L is the Langmuir equilibrium constant (L mg^{-1}).

The Langmuir plots of $\frac{C_e}{q_e}$ vs C_e for the adsorption of both AR1 and AR42 provided straight lines with high correlation coefficients (R^2). The values of Langmuir parameters are represented in Table 3.

In order to describe the adsorption process, a dimensionless constant (separation factor) is defined as R_L . It describes that the adsorption process is irreversible when R_L is 0; favorable when R_L is between 0 and 1, linear when R_L is 1, and unfavorable when R_L is higher than 1. R_L is described as Eq. (4):

$$R_L = \frac{1}{1 + K_L C_0} \tag{4}$$

where K_L is the Langmuir constant (L mg^{-1}), and C_0 is the initial concentration of dye (mg L^{-1}). Table 3 also represents the values of R_L .

3.3.2. Temkin isotherm

The Temkin isotherm equation describes that the heat of adsorption of all the molecules decreases linearly with the coverage due to the adsorbent–adsorbate interactions [59]. The Temkin linear equation is written as Eq. (5) [58,59]:

$$q_e = B \ln K_T + B \ln C_e \tag{5}$$

where $B = RT/b$, T is the absolute temperature (K) and R is the gas constant ($8.314 \text{ J K}^{-1} \text{ mol}^{-1}$). The values of

Table 3
Isotherm parameters for the adsorption of AR1 and AR42 onto HNTs- G_3

Dye	Langmuir				Temkin			Freundlich		
	Q_m (mg g^{-1})	K_L (L mg^{-1})	R_L	R^2	B	K_T	R^2	K_F (mg L^{-1}) n^{-1}	n	R^2
AR42	120.48	0.17	0.037–0.18	0.979	49.511	1.6	0.898	31.97	3.13	0.863
AR1	129.87	0.27	0.006–0.12	0.972	20.135	7.15	0.881	45.86	4.18	0.887

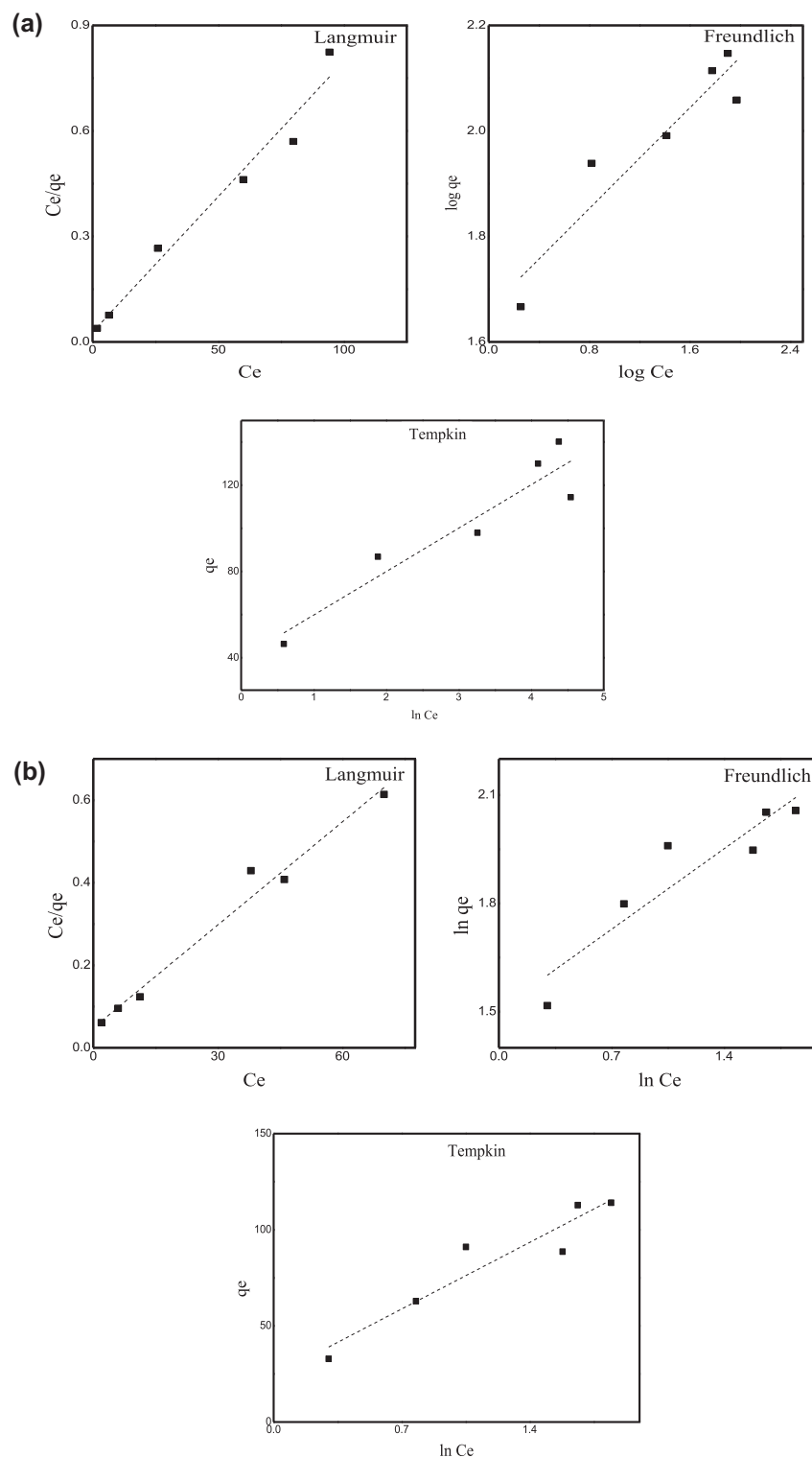


Fig. 10. Adsorption isotherm of AR1 and AR42 onto HNT-G₃ at different initial dye concentrations: (a) AR1 and (b) AR42.

B and K_T are calculated from the plot of q_e vs. $\ln C_e$ and Table 3 illustrates the value of these constants. The low correlation coefficient shows the unfit relation of experimental data with Temkin isotherm.

3.3.3. Freundlich isotherm

Another popular isotherm for dye adsorption onto a heterogeneous surface is the Freundlich isotherm model [58]. Linear form of Freundlich equation is shown as Eq. (6):

$$\log q_e = \log K_F + \frac{1}{n} \log C_e \quad (6)$$

K_F and $\frac{1}{n}$ were determined from the plot of $\log q_e$ vs $\log C_e$ where K_F illustrates the adsorption capacity and $1/n$ is related to the adsorption strength. The values of Freundlich constants are represented in Table 3. According to Table 3, the low R^2 values of this model show its inapplicability for AR1 and AR42 experimental data. The isotherm plots are drawn in Fig. 10, and the results indicate that the adsorption of AR1 and AR14 on HNTs-G₃ follows the Langmuir model with the highest R^2 value. This result shows that adsorption on the modified HNTs via terminated amine groups follows the monolayer adsorption format.

3.4. Kinetic studies

The adsorption kinetic explains the rate of adsorption. In order to study the adsorption mechanism the pseudo-first-order, pseudo-second-order, and intraparticle diffusion models are studied and fitted to the experimental data [51].

3.4.1. Pseudo-first-order model

The linear form of the pseudo-first-order equation can be shown as Eq. (7) [58]:

$$\log(q_e - q_t) = \log(q_e) - \frac{k_1}{2.303t} \quad (7)$$

where q_e and q_t (mg g^{-1}) are the amount of dye adsorbed at equilibrium and time t (min), respectively, and k_1 (min^{-1}) is the pseudo-first-order rate constant. The kinetic constant were calculated from the plot of $\log(q_e - q_t)$ vs t . The difference between the experimental and calculated q_e illustrated the inapplicability of the model, despite the high correlation coefficients.

3.4.2. Pseudo-second-order model

Another well-known kinetic model is pseudo-second-order model. The linear form of this model is presented as Eq. (8):

$$\frac{t}{q_t} = \frac{1}{k_2 q_e^2} + \left(\frac{1}{q_e}\right)t \quad (8)$$

where k_2 is the pseudo-second-order rate constant ($\text{g mg}^{-1} \text{min}^{-1}$). q_e and k_2 can be calculated from the plot of $\frac{t}{q_t}$ vs t . The initial adsorption rates can be evaluated by Eq. (9) [58]:

$$h_{0,2} = k_2 q_e^2 \quad (9)$$

The results show high rates of adsorption at initial times, and this quick adsorption can be related to the enrichment in the mass transportation driving force emerged from anionic dye to the available adsorption sites. According to the results in Table 4, at higher dye concentrations, because of agglomeration or dimerization, the adsorption rate reduces compared to the lower initial dye concentrations [58].

3.4.3. Intraparticle diffusion model

Adsorption process of dye from aqueous phase onto porous materials is usually controlled by film diffusion or intraparticle diffusion rate. Eq. (10) illustrates this mechanism:

$$q_t = K_{\text{dif}} t^{\frac{1}{2}} + C \quad (10)$$

where K_{dif} is the intraparticle diffusion rate constant ($\text{mg g}^{-1} \text{min}^{-0.5}$) and C is the intercept (mg g^{-1}), which illustrates the thickness of the layer. High value of C and intercept represents a notable effect of boundary layer [51,58], and the greater boundary layer effect. If q_t vs $t^{1/2}$ is linear and if the plot passes through the origin, then the rate-limiting process will only be certain by intraparticle diffusion model [60]. The plots indicating the adsorption kinetic are represented in Fig. 11. The fitted kinetic models to the experimental data demonstrated that the adsorption process followed the pseudo-second-order kinetic model.

3.5. Thermodynamic studies

The adsorption capacity of acidic dyes onto HNT-G₃ was found to decrease via increasing the temperature.

Table 4
Kinetic parameters for the adsorption of AR1 and AR42 onto HNTs-G₃

Dye	C ₀ (mg L ⁻¹)	Pseudo-first-order			Pseudo-second-order			Intraparticle diffusion				
		q _e (mg g ⁻¹)	q _{e(c)} (mg g ⁻¹)	k ₁ (min ⁻¹)	R ²	q _e (mg g ⁻¹)	k ₂ (g mg ⁻¹ min ⁻¹)	t _{0.2}	R ²	C (mg g ⁻¹)	K _{dif} (mg g ⁻¹ min ^{-0.5})	R ²
AR1	25	46.39	2.6	0.039	0.21	46.51	0.25	540.8	0.999	21.6	4.3	0.48
	50	86.6	4.29	0.037	0.21	93.45	0.008	69	0.985	38.3	8.8	0.54
	75	97.95	24.07	0.072	0.55	135.2	0.0005	9.13	0.727	13.3	14.7	0.72
	100	114.4	8.6	0.05	0.36	125	0.0005	7.8	0.996	47.4	12.3	0.60
	125	117	16.84	0.06	0.53	126	0.008	127	0.999	46.76	13.03	0.63
	150	156.18	4.02	0.034	0.21	126.58	0.008	128	0.999	62.9	17.2	0.62
AR42	25	32.8	2.89	0.026	0.217	33.7	0.09	102.2	0.999	14.84	3.21	0.52
	50	62.85	5.00	0.038	0.347	66.2	0.032	141.9	0.999	28.12	6.41	0.54
	75	91.07	9.11	0.05	0.458	106.3	0.98	11090.37	1	50.43	9.12	0.46
	100	85.5	16.11	0.064	0.556	104.1	0.004	43.39	0.995	27.96	11.71	0.76
	125	112.5	19.95	0.068	0.556	123	0.005	75.64	0.997	29.46	16.09	0.78
	150	132.8	22.9	0.07	0.556	156.2	0.003	73.19	0.996	41.9	17.56	0.76

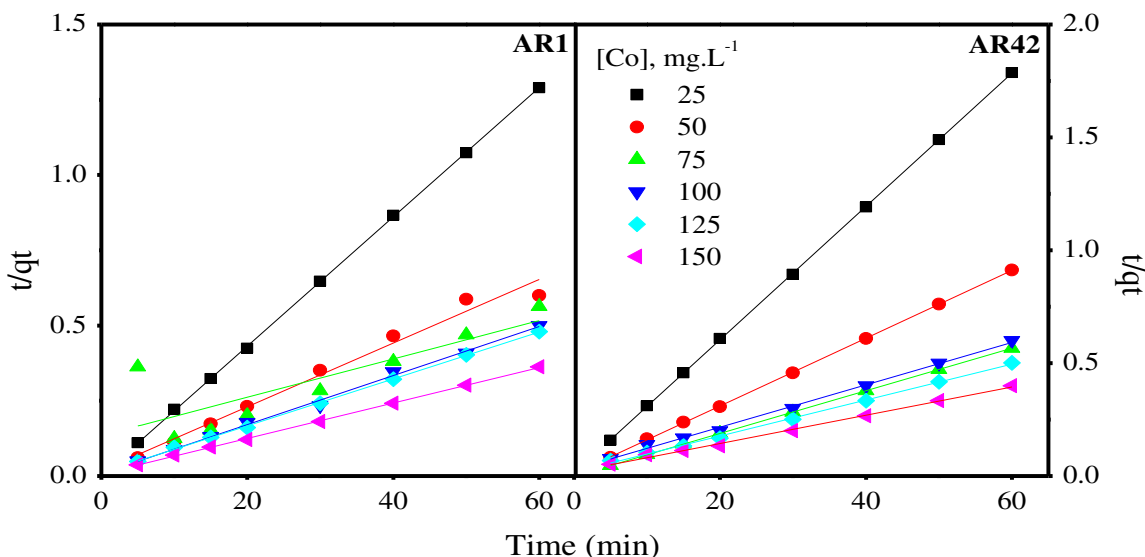


Fig. 11. Pseudo-second-order adsorption kinetic of AR1 and AR42 onto HNT-G₃ at different initial dye concentrations.

Table 5
Thermodynamic parameters of AR1 and AR42 adsorption on HNTs-G₃

Dye	q_e (mg g ⁻¹)	T (K)	ΔG° (kJ mol ⁻¹)	ΔH° (kJ mol ⁻¹)	ΔS° (kJ mol ⁻¹ K ⁻¹)
AR1	46.5	298	-8,126.03	-35,633	-93.572
	44.4	308	-7,076.84		
	41.75	318	-6,119.55		
	31	328	-3,225.2		
	32.8	338	-3,761.83		
	33.8	348	-4,143.89		
AR42	32.85	298	-6,934.78	-21,283	-51.059
	29.64	308	-4,973.68		
	28.21	318	-4,445.9		
	27.5	328	-4,267.7		
	27.4	338	-4,359.8		
	27.7	348	-3,764.5		

The removal efficiency decreased from 94 and 93.03% for AR42 and AR1 at 298 K to 80–85.6% at 328 K. This means that the dye affinity to adsorbent was more desirable at lower temperatures. The quantity of AR1 and AR42 adsorbed on HNTs-G₃ at equilibrium at 298, 308, 318, 328, 338, and 348 K are determined and reported in Table 5. Thermodynamic parameters including the change of Gibbs free energy (ΔG° , kJ mol⁻¹), enthalpy (ΔH° , kJ mol⁻¹), and entropy (ΔS° , kJ mol⁻¹ K⁻¹) are calculated from Eqs. (11) and (12) [43,58,61]:

$$\Delta G^\circ = -RT \ln K_L \tag{11}$$

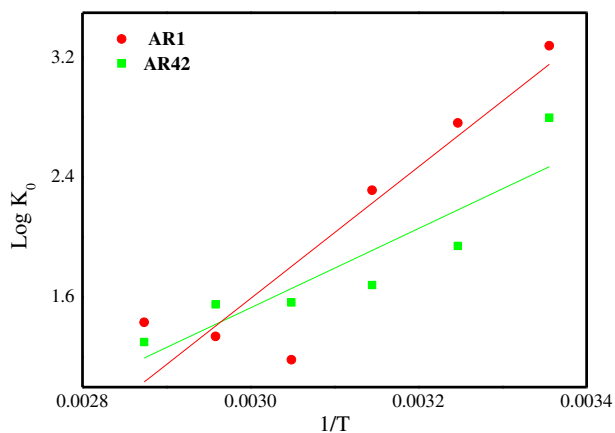


Fig. 12. Van't Hoff plots of AR1 and AR42 adsorption onto HNT-G₃.

Table 6
Comparison of adsorption capacities of various acidic dyes onto different adsorbents

Adsorbent	Maximum adsorption capacity Q_m (mg g ⁻¹)	Adsorbate	pH	Dye concentration (mg L ⁻¹)	Solution volume (mL)	Adsorbent (g L ⁻¹)	Refs.
Al/CTAB-bentonite	42.37–47.55	MO	>3	100	–	0.5 (g)	[63]
Hexadecyltrimethylammonium bromide-HNTs	91.74	MO	6.7	100	50	2	[51]
Cetyltrimethylammonium bromide–bentonite	30.28	Acid Scarlet GR	7.5	50	100	2	[64]
Polydiallyldimethylammonium–bentonite	42.72	Acid Scarlet GR	7.5	50	100	2	[64]
Cetyltrimethylammonium bromide–bentonite	24.85	Acid Dark Blue 2G	7.9	50	100	2	[64]
Polydiallyldimethylammonium–bentonite	33.34	Acid Dark Blue 2G	7.9	50	100	2	[64]
Polyepichlorohydrindimethylamine–bentonite	45.54	Acid Scarlet GR	7.5	50	100	2	[64]
Polyepichlorohydrindimethylamine–bentonite	35.93	Acid Dark Blue 2G	7.9	50	100	2	[64]
Coal fly ash	92.5–103.09	AR1	6	400	100	1	[54]
Coal fly ash –600	32.79–52.63	AR1	6	400	100	1	[54]
Coal fly ash –NaOH	12.66–25.12	AR1	6	400	100	1	[54]
HNTs-Fe ₃ O ₄	0.65	MO	–	300	–	2	[52]
HNTs-G ₃	120.48	AR42	3	25	250	0.7	This study
HNTs-G ₃	129.87	AR1	3	25	250	0.5	This study

$$\Delta G^\circ = \Delta H^\circ - T\Delta S^\circ \quad (12)$$

$$\ln K_0 = \frac{\Delta S^\circ}{R} - \frac{\Delta H^\circ}{RT} \quad (13)$$

where K_L is the Langmuir constant, R is the universal gas constant, and T is the absolute temperature (K). The values of ΔH° and ΔS° can be obtained from the slope and intercept of the plot of ΔG° against T . The calculated free energy changes (ΔG°) are negative, which shows that the adsorption is spontaneous, but ΔG° did not increase regularly with increasing the temperature in case of AR42, which reveals that the adsorption of AR42 onto HNT-G₃ did not follow a clear policy at high temperature [43]. The values of enthalpy and entropy change can also be calculated from the Van't Hoff equation as Eq. (13):

The slope and intercept of Eq. (13) equal to $(-\frac{\Delta H^\circ}{R})$ and $(\frac{\Delta S^\circ}{R})$. The negative values of ΔH° and ΔS° illustrate the exothermic adsorption process, and the increase of orderliness and organization [43,59]. The Van't Hoff plots of AR1 and AR42 onto HNT-G₃ and the calculated thermodynamic values are shown in Fig. 12 and Table 5. Results demonstrated that negative values of ΔG° for AR1 were greater than AR42. The difference between the mentioned dyes is related to the number of sulfonate groups. Dye structure containing more sulfonate groups possesses stronger attraction compared to the dye with less sulfonate groups.

3.6. Comparative study

Different mineral adsorbents used for the removal of anionic dyes from solutions have been reported in Table 6 and their maximum adsorption capacities (Q_m) have been compared to each other. It should be noted that the maximum adsorption capacity of each adsorbent has been achieved at different conditions. However, Table 6 reveals that HNTs-G₃ synthesized in this study has the highest adsorption capacities of 120.48–129.87 (mg g⁻¹) for the removal of AR42 and AR1, respectively. The results of using coal fly ash as a non-mineral adsorbent for the removal of AR1 have also been reported in Table 6 in order to compare with the results of the present study. It can be seen that HNT-G₃ at lower dosages and lower initial concentration of AR1 has reached a higher adsorption capacity of 129.87 (mg g⁻¹) compared to coal fly ash with Q_m of 103.09 (mg g⁻¹).

4. Conclusion

In the present study, the surface of HNTs were successfully modified with dendrimer via divergent synthesis route, enabling its application in various research areas such as nanocomposites, enzyme immobilization, controlled release, and pollutant extraction. In order to synthesize the generation 3 of HNTs (HNTs-G₃), they were first purified and amine functionalized by HCl solution (35%) and 3-Aminepropyl triethoxysilane (APTES), respectively. Then, by employing the successive Michael addition of MA and amidation with EDA, the dendritic structure is synthesized onto the amine groups of APTES (generation 1). Finally, by repeating the latter steps, HNTs-G₃ was synthesized. FTIR and EDS analysis confirmed the successful functionalization process, and FESEM images indicated no deformation in the surface morphology of HNTs. The application of the synthesized HNTs-G₃ as an adsorbent was evaluated for the removal of two acid dyes: AR1 and AR42. The effect of key parameters including dendrimer generation, pH, adsorbent dosage, initial dye concentration, temperature, and time was studied on the adsorption performance. Experimental results illustrated that the raw HNTs just reached the low values of 9–13.8% for the removal of AR1 and AR42. But, after the modification process the experimental outcomes indicated that the equilibrium was rapidly integrated after 15 min of contact time, and considerably higher removal efficiencies (94% for AR1 and 87% for AR42) were obtained at pH 3 due to the strong electrostatic attraction forces between the negatively charged dye molecules and positive amine groups of HNTs-G₃. The isotherm,

kinetic, and thermodynamic parameters were also investigated and the fitted data explored that the adsorption process had followed the Langmuir isotherm and pseudo-second-order kinetic equation. Thermodynamic studies also revealed that the adsorption process using HNTs-G₃ was an exothermic and spontaneous process. The obtained high removal efficiencies of HNTs-G₃ can suggest the functionalized HNTs as an efficient and effective adsorbent for the removal of organic dye molecules from the polluted wastewaters.

References

- [1] Y.M. Lvov, D.G. Shchukin, H. Möhwald, R.R. Price, Halloysite clay nanotubes for controlled release of protective agents, *ACS Nano* 2(5) (2008) 814–820.
- [2] J. Zhang, D. Zhang, A. Zhang, Z. Jia, D. Jia, Dendritic polyamidoamine-grafted halloysite nanotubes for fabricating toughened epoxy composites, *Iran. Polym. J.* 22(7) (2013) 501–510.
- [3] P. Luo, J.-S. Zhang, B. Zhang, J.-H. Wang, Y.-F. Zhao, J.-D. Liu, Preparation and characterization of silane coupling agent modified halloysite for Cr(VI) removal, *Ind. Eng. Chem. Res.* 50(17) (2011) 10246–10252.
- [4] E. Abdullayev, Y. Lvov, Halloysite clay nanotubes as a ceramic “skeleton” for functional biopolymer composites with sustained drug release, *J. Mater. Chem. B* 1 (23) (2013) 2894–2903.
- [5] D. Banaś, A. Kubala-Kukuś, J. Braziewicz, U. Majewska, M. Pajek, J. Wudarczyk-Moćko, K. Czech, M. Garnuszek, P. Słomkiewicz, B. Szczepanik, Study of properties of chemically modified samples of halloysite mineral with X-ray fluorescence and X-ray powder diffraction methods, *Radiat. Phys. Chem.* 93 (2013) 129–134.
- [6] R. Li, Z. Hu, S. Zhang, Z. Li, X. Chang, Functionalized halloysite nanotubes with 2-hydroxybenzoic acid for selective solid-phase extraction of trace iron(III), *Int. J. Environ. Anal. Chem.* 93(7) (2013) 767–779.
- [7] S. Sahnoun, M. Boutahala, H. Zaghoulane-Boudiaf, L. Zerroual, Trichlorophenol removal from aqueous solutions by modified halloysite: Kinetic and equilibrium studies, *Desalin. Water Treat.* (ahead-of-print) (2015) 1–11.
- [8] D.-Y. Lei, B. Li, Q. Wang, B. Wu, L. Ma, H. Xu, Removal of neutral red from aqueous solution using pleurotus ostreatus nanoparticles by response surface methodology, *Desalin. Water Treat.* (ahead-of-print) 54 (10) (2014) 1–12.
- [9] E. Joussein, S. Petit, B. Delvaux, Behavior of halloysite clay under formamide treatment, *Appl. Clay Sci.* 35(1–2) (2007) 17–24.
- [10] W.O. Yah, A. Takahara, Y.M. Lvov, Selective modification of halloysite lumen with octadecylphosphonic acid: New inorganic tubular micelle, *J. Am. Chem. Soc.* 134(3) (2012) 1853–1859.
- [11] J.D.D. Melo, A.P.C. Barbosa, M.C.B. Costa, G.N. de Melo, Encapsulation of solvent into halloysite nanotubes to promote self-healing ability in polymers, *Adv. Compos. Mater.* 23(5–6) (2014) 507–519.

- [12] P. Pasbakhsh, H. Ismail, M.A. Fauzi, A.A. Bakar, EPDM/modified halloysite nanocomposites, *Appl. Clay Sci.* 48(3) (2010) 405–413.
- [13] S. Wang, C.W. Ng, W. Wang, Q. Li, L. Li, A comparative study on the adsorption of acid and reactive dyes on multiwall carbon nanotubes in single and binary dye systems, *J. Chem. Eng. Data* 57(5) (2012) 1563–1569.
- [14] F. Zhang, B. Wang, S. He, R. Man, Preparation of graphene-oxide/polyamidoamine dendrimers and their adsorption properties toward some heavy metal ions, *J. Chem. Eng. Data* 59(5) (2014) 1719–1726.
- [15] R. Zhai, B. Zhang, L. Liu, Y. Xie, H. Zhang, J. Liu, Immobilization of enzyme biocatalyst on natural halloysite nanotubes, *Catal. Commun.* 12(4) (2010) 259–263.
- [16] J. Tully, R. Yendluri, Y. Lvov, Halloysite clay nanotubes for enzyme immobilization, *Biomacromolecules* 17(2) (2015) 615–621.
- [17] P. Pasbakhsh, G.J. Churchman, J.L. Keeling, Characterisation of properties of various halloysites relevant to their use as nanotubes and microfibre fillers, *Appl. Clay Sci.* 74 (2013) 47–57.
- [18] Y. Chen, Y. Zhang, J. Liu, H. Zhang, K. Wang, Preparation and antibacterial property of polyethersulfone ultrafiltration hybrid membrane containing halloysite nanotubes loaded with copper ions, *Chem. Eng. J.* 210 (2012) 298–308.
- [19] H. Yu, Y. Zhang, X. Sun, J. Liu, H. Zhang, Improving the antifouling property of polyethersulfone ultrafiltration membrane by incorporation of dextran grafted halloysite nanotubes, *Chem. Eng. J.* 237 (2014) 322–328.
- [20] P. Huo, X. Gao, Z. Lu, X. Liu, Y. Luo, W. Xing, J. Li, Y. Yan, Photocatalytic degradation of antibiotics in water using metal ion@ TiO₂/HNTs under visible light, *Desalination and Water Treatment* 52(37–39) (2014) 6985–6995.
- [21] T. Yang, M. Du, M. Zhang, H. Zhu, P. Wang, M. Zou, Synthesis and immobilization of Pt nanoparticles on amino-functionalized halloysite nanotubes toward highly active catalysts, *Nanomater. Nanotechnol.* 5 (2015).
- [22] Q. Peng, M. Liu, J. Zheng, C. Zhou, Adsorption of dyes in aqueous solutions by chitosan–halloysite nanotubes composite hydrogel beads, *Microporous Mesoporous Mater.* 201 (2015) 190–201.
- [23] W. Xu, B. Luo, W. Wen, W. Xie, X. Wang, M. Liu, C. Zhou, Surface modification of halloysite nanotubes with l-lactic acid: An effective route to high-performance poly (l-lactide) composites, *J. Appl. Polym. Sci.* 132(7) (2015).
- [24] W. Jinhua, Z. Xiang, Z. Bing, Z. Yafei, Z. Rui, L. Jindun, C. Rongfeng, Rapid adsorption of Cr(VI) on modified halloysite nanotubes, *Desalination* 259(1–3) (2010) 22–28.
- [25] P. Yuan, P.D. Southon, Z. Liu, M.E. Green, J.M. Hook, S.J. Antill, C.J. Kepert, Functionalization of halloysite clay nanotubes by grafting with γ -Aminopropyltriethoxysilane, *J. Phys. Chem. C* 112(40) (2008) 15742–15751.
- [26] S. Riela, M. Massaro, C.G. Colletti, A. Bommarito, C. Giordano, S. Milioto, R. Noto, P. Poma, G. Lazzara, Development and characterization of co-loaded curcumin/triazole-halloysite systems and evaluation of their potential anticancer activity, *Int. J. Pharm.* 475(1–2) (2014) 613–623.
- [27] Q. Hu, S. Qiao, F. Haghseresht, M. Wilson, G. Lu, Adsorption study for removal of basic red dye using bentonite, *Ind. Eng. Chem. Res.* 45(2) (2006) 733–738.
- [28] P. Yuan, P.D. Southon, Z. Liu, C.J. Kepert, Organosilane functionalization of halloysite nanotubes for enhanced loading and controlled release, *Nanotechnology* 23(37) (2012) 375705.
- [29] H. Chen, J. Zhao, J. Wu, H. Yan, Selective desorption characteristics of halloysite nanotubes for anionic azo dyes, *RSC Adv.* 4(30) (2014) 15389–15393.
- [30] L. Eskandarian, M. Arami, E. Pajootan, Evaluation of adsorption characteristics of multiwalled carbon nanotubes modified by a poly (propylene imine) dendrimer in single and multiple dye solutions: Isotherms, kinetics, and thermodynamics, *J. Chem. Eng. Data* 59(2) (2014) 444–454.
- [31] O. Nowacka, K. Milowska, M. Bryszewska, Interaction of PAMAM dendrimers with bovine insulin depends on nanoparticle end-groups, *J. Lumin.* 162 (2015) 87–91.
- [32] R.W. Scott, O.M. Wilson, R.M. Crooks, Synthesis, characterization, and applications of dendrimer-encapsulated nanoparticles, *J. Phys. Chem. B* 109(2) (2005) 692–704.
- [33] M. Brik, P. Schoeberl, B. Chamam, R. Braun, W. Fuchs, Advanced treatment of textile wastewater towards reuse using a membrane bioreactor, *Process Biochem.* 41 (2006) 1751–1757.
- [34] N.S.A. Mutamim, Z.Z. Noor, M.A. Abu Hassan, G. Olsson, Application of membrane bioreactor technology in treating high strength industrial wastewater: A performance review, *Desalination* 305 (2012) 1–11.
- [35] R. Jiratananon, A. Sungpet, P. Luangsowan, Performance evaluation of nanofiltration membranes for treatment of effluents containing reactive dye and salt, *Desalination* 130 (2000) 177–183.
- [36] A.M. Lotito, U. Fratino, G. Bergna, D.C. Iaconi, Integrated biological and ozone treatment of printing textile wastewater, *Chem. Eng. J.* 195–196 (2012) 261–269.
- [37] A.K. Verma, R.R. Dash, P. Bhunia, A review on chemical coagulation/flocculation technologies for removal of colour from textile wastewaters, *J. Environ. Manage.* 93 (2012) 154–168.
- [38] R. Ordóñez, A. Moral, D. Hermosilla, A. Blanco, Combining coagulation, softening and flocculation to dispose reverse osmosis retentates, *J. Ind. Eng. Chem.* 18 (2012) 926–933.
- [39] A. Aouni, C. Fersi, B. Cuartas-Urbe, A. Bes-Pía, M.I. Alcaina-Miranda, M. Dhahbi, Reactive dyes rejection and textile effluent treatment study using ultrafiltration and nanofiltration processes, *Desalination* 297 (2012) 87–96.
- [40] C. Huang, C. Dong, Z. Tang, Advanced chemical oxidation: Its present role and potential future in hazardous waste treatment, *Waste Manage.* 13(5–7) (1993) 361–377.
- [41] J. Basiri Parsa, S. Hagh Negahdar, Treatment of wastewater containing acid blue 92 dye by advanced ozone-based oxidation dation methods, *Sep. Purif. Technol.* 98 (2012) 315–320.
- [42] J.C. Moreno-Piraján, L. Giraldo, Heavy metal ions adsorption from wastewater using activated carbon from orange peel, *J. Chem.* 9(2) (2012) 926–937.

- [43] G. Kiani, M. Dostali, A. Rostami, A.R. Khataee, Adsorption studies on the removal of malachite green from aqueous solutions onto halloysite nanotubes, *Appl. Clay Sci.* 54(1) (2011) 34–39.
- [44] G. Crini, Non-conventional low-cost adsorbents for dye removal: A review, *Bioresour. Technol.* 97(9) (2006) 1061–1085.
- [45] A. Ip, J. Barford, G. McKay, Reactive black dye adsorption/desorption onto different adsorbents: Effect of salt, surface chemistry, pore size and surface area, *J. Colloid Interface Sci.* 337(1) (2009) 32–38.
- [46] V.K. Gupta, R. Jain, M.N. Siddiqui, T.A. Saleh, S. Agarwal, S. Malati, D. Pathak, Equilibrium and thermodynamic studies on the adsorption of the dye rhodamine-B onto mustard cake and activated carbon, *J. Chem. Eng. Data* 55(11) (2010) 5225–5229.
- [47] M. Ahmed, R. Ram, Removal of basic dye from waste-water using silica as adsorbent, *Environ. Pollut.* 77(1) (1992) 79–86.
- [48] D. Karadag, E. Akgul, S. Tok, F. Erturk, M.A. Kaya, M. Turan, Basic and reactive dye removal using natural and modified zeolites, *J. Chem. Eng. Data* 52(6) (2007) 2436–2441.
- [49] V. Gupta, Application of low-cost adsorbents for dye removal—A review, *J. Environ. Manage.* 90(8) (2009) 2313–2342.
- [50] M. Toor, B. Jin, Adsorption characteristics, isotherm, kinetics, and diffusion of modified natural bentonite for removing diazo dye, *Chem. Eng. J.* 187 (2012) 79–88.
- [51] R. Liu, K. Fu, B. Zhang, D. Mei, H. Zhang, J. Liu, Removal of methyl orange by modified halloysite nanotubes, *J. Dispersion Sci. Technol.* 33(5) (2012) 711–718.
- [52] Y. Xie, D. Qian, D. Wu, X. Ma, Magnetic halloysite nanotubes/iron oxide composites for the adsorption of dyes, *Chem. Eng. J.* 168(2) (2011) 959–963.
- [53] M. Albdiry, B. Yousif, Role of silanized halloysite nanotubes on structural, mechanical properties and fracture toughness of thermoset nanocomposites, *Mater. Des.* 57 (2014) 279–288.
- [54] T.-C. Hsu, Adsorption of an acid dye onto coal fly ash, *Fuel* 87(13–14) (2008) 3040–3045.
- [55] Y. Wong, Y. Szeto, W. Cheung, G. McKay, Equilibrium studies for acid dye adsorption onto chitosan, *Langmuir* 19(19) (2003) 7888–7894.
- [56] M. Anbia, S. Salehi, Removal of acid dyes from aqueous media by adsorption onto amino-functionalized nanoporous silica SBA-3, *Dyes Pigm.* 94(1) (2012) 1–9.
- [57] R. Liu, B. Zhang, D. Mei, H. Zhang, J. Liu, Adsorption of methyl violet from aqueous solution by halloysite nanotubes, *Desalination* 268(1–3) (2011) 111–116.
- [58] F. Nekouei, S. Nekouei, I. Tyagi, V.K. Gupta, Kinetic, thermodynamic and isotherm studies for acid blue 129 removal from liquids using copper oxide nanoparticle-modified activated carbon as a novel adsorbent, *J. Mol. Liq.* 201 (2015) 124–133.
- [59] N. Oladoja, C. Aboluwoye, Y. Oladimeji, Kinetics and isotherm studies on methylene blue adsorption onto ground palm kernel coat, *Turk. J. Eng. Environ. Sci.* 32(5) (2009) 303–312.
- [60] M. Liu, J. Xu, B. Cheng, W. Ho, J. Yu, Synthesis and adsorption performance of Mg(OH)₂ hexagonal nanosheet-graphene oxide composites, *Appl. Surf. Sci.* (2015).
- [61] H. Kim, S.-O. Kang, S. Park, H.S. Park, Adsorption isotherms and kinetics of cationic and anionic dyes on three-dimensional reduced graphene oxide macrostructure, *J. Ind. Eng. Chem.* 21 (2015) 1191–1196.
- [62] M.C. Popescu, D. Filip, C. Vasile, C. Cruz, J. Rueff, M. Marcos, J. Serrano, G. Singurel, Characterization by fourier transform infrared spectroscopy (FT-IR) and 2D IR correlation spectroscopy of PAMAM dendrimer, *J. Phys. Chem. B* 110(29) (2006) 14198–14211.
- [63] J. Wang, H. Ma, W. Yuan, W. He, S. Wang, J. You, Synthesis and characterization of an inorganic/organic-modified bentonite and its application in methyl orange water treatment, *Desalin. Water Treat.* 52(40–42) (2014) 7660–7672.
- [64] Q. Li, Q.-Y. Yue, Y. Su, B.-Y. Gao, H.-J. Sun, Equilibrium, thermodynamics and process design to minimize adsorbent amount for the adsorption of acid dyes onto cationic polymer-loaded bentonite, *Chem. Eng. J.* 158(3) (2010) 489–497.